Springer

KSME

Journal of Mechanical Science and Technology 24 (2) (2010) 593~599
www.springerlink.com/content/1738-494x
DOI 10.1007/s12206-009-1215-5

Numerical investigation of transient side-loads in the start-up process of a rocket nozzle †

Vincent Lijo[1], Heuy Dong Kim[1,*], Toshiaki Setoguchi[2] and Shigeru Matsuo[2]

[1]*School of Mechanical Engineering, Andong National University, Andong, 760-749, Korea*
[2]*Department of Mechanical Engineering, Saga University, 1, Honjo, Saga, Japan*

(Manuscript Received March 19, 2009; Revised September 17, 2009; Accepted September 24, 2009)

Abstract

A numerical investigation of transient side-loads in axisymmetric over-expanded thrust optimized contour nozzles is presented. These nozzles experience side-loads during start-up and shut-down operations because of flow separation at the nozzle walls. Two types of flow separations, FSS and RSS shock structures, also occur. A two-dimension numerical simulation was carried out over axisymmetric TOC nozzles to validate the present results and investigate oscillatory flow characteristics for start-up processes. Reynolds Averaged Navier-Stokes equations are numerically solved using a fully implicit finite volume scheme. Governing equations are solved via the coupled implicit scheme. The Reynolds Stress turbulence model is selected for this work. It was found that the present computed pressure at the nozzle walls closely matched the experimental data. The phenomenon of hysteresis was also observed between these two shock structures. The transition from an FSS to RSS pattern during the start-up process showed maximum nozzle wall pressure and fluctuations in shear stress values. Oscillatory pressure was observed on the nozzle walls with high pressure ratio. The present results show that the magnitude of nozzle wall pressure variation is high for the phenomenon of oscillation.

Keywords: Free shock separation; Over-expansion flow; Restricted shock separation; Side-loads; Supersonic nozzle

1. Introduction

A large scale launch vehicle requires a nozzle which can produce maximum specific impulse and thrust with reduced nozzle length. Various supersonic nozzles, such as Thrust Optimized Contour (TOC) and Compressed Truncated Perfect (CTP) contours, have been developed to meet such demands. TOC nozzles are currently used in Vulcain, Space Shuttle Main Engine (SSME), or J2S launcher engines. These rocket engines experience long periods of over-expanded operation with flow separation in a transient phase at engine start-up or shut-down. In general, two separation patterns are observed: shock separation (FSS) and restricted shock separation (RSS) [1]. The FSS structure can be observed in various types of nozzles, such as conical contour nozzles and bell type nozzles, including TP, TOC, and CTP nozzles. In FSS, the flow separates fully from the nozzle wall due to an oblique shock that originates from the nozzle wall and is directed towards the nozzle centerline. The separated shear layer continues as a free jet (Fig. 1). Since no reattachment occurs down the separation location, this separation flow pattern is termed as free shock separation. Downstream from the separation location, a back flow region exists where ambient air is sucked into the nozzle due to the entrainment effect of the separated jet flow [2]. The nozzle flow thus fully separates from the wall at a certain ratio of wall to ambient pressure.

RSS is a peculiar type of separation pattern observed only in TOC and CTP nozzles at a certain range of pressure ratios. In RSS, the flow separation is restricted over a short axial distance. The separated shear layer reattaches to the nozzle wall, thus generating shocks and expansion waves. Due to the very short separated region, this flow regime is called restricted shock separation (Fig. 2) [2]. The reattached flow results in wall pressures above ambient, which can initiate unsteady side-loads depending upon the asymmetry of the overall flow pattern, and the oscillatory behavior of the associated shock system. The RSS separation pattern exists in nozzles which experience internal shock because of the large divergent angle of the nozzle wall. However, the presence of an internal shock in the nozzle does not mean that RSS flow conditions will appear ubiquitous. Both FSS and RSS can exist in such nozzles at different operating conditions. According to a previous work [1], it is known that the separation pattern evolves from FSS to RSS when the pressure ratio increases. Transitions

† This paper was recommended for publication in revised form by Associate Editor Do Hyung Lee
*Corresponding author. Tel.: +82 54 820 5622, Fax.: +82 54 820 6127
E-mail address: kimhd@andong.ac.kr

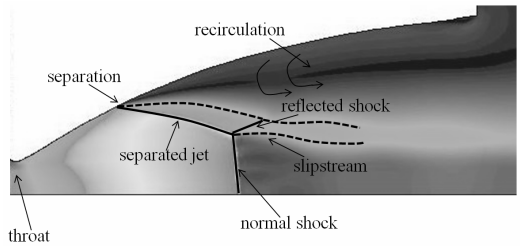

Fig. 1. Free shock separation pattern (Ref. [2]).

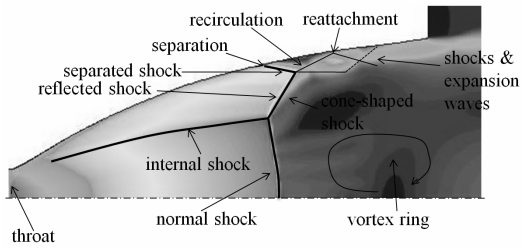

Fig. 2. Restricted shock separation (Ref. [2]).

between these two kinds of separation patterns result in the hysteresis phenomenon. High peaks of side-loads are observed during transitions from FSS to RSS and vice versa. This hysteresis phenomenon appears typical during the start-up and the shut-down processes. Also, FSS to RSS transition is rather fast, and the total impulse communicated to the nozzle wall will therefore be limited by the short duration of this phenomenon. The essential mechanisms that cause FSS and RSS phenomena in propulsion nozzles are due to shock boundary layer interactions, as described in many previous researches. In the present study, we focus on the FSS/RSS and their transitions, which can be influenced by many parameters, such as boundary layer characteristics, nozzle geometry, pressure ratio, thermal conditions of nozzle wall, working gas, turbulence, etc. The present work does not take into account gas temperature effects.

Nguyen et al. [3] highlighted an uncommon phenomenon observed at high pressure ratios for TOC nozzles. At high pressure ratios, the separation structure repeatedly moves downstream and upstream of the nozzle resulting in the oscillation of nozzle wall pressure. Chen et al. [4] first observed the reattached flow in their numerical simulations, and showed the presence of a trapped vortex immediately downstream of the central normal shock. Soon after, Nasuti et al. [5] and Onofri et al. [6] explained that an inviscid mechanism causes the generation of the vortex, which generates side-loads. Frey et al. [7, 8] showed the existence of a specific cap shock pattern, which is a key driver for the transition from FSS to RSS and vice versa [9, 10]. They observed that irregular movements of oblique separation shock and the cap shock pattern, relative to each other, are responsible for the initiation of flow transitions [11]. On the other hand, Nguyen et al. [3] showed the end-effects which induce very high levels of fluctuation. These experimental findings were numerically reconfirmed by Nebbache et al. [12]. The rocket engine transient side-load is a very complicated problem because it is a strongly unstable process. Morinigo et al. [13] first captured the phenomenon of cyclic transition between reattached and non-reattached flow separation modes. They also confirmed the role of separation bubble dynamics in high side-load peaks. According to Hagemann et al. [14], momentum balance across the cap-shock pattern, with the radial momentum toward the wall generated by the reflected internal shock, causes the re-attachment. Nasuti et al. [15] explained that flow reattachment to the wall depended on the values and type of upstream pressure gradient, regardless of the existence of internal shock.

The literature review above shows that rocket nozzles demonstrate the hysteresis effect, the transition of FSS to RSS, and the oscillation of nozzle wall pressures at high pressure ratios. Numerical and experimental studies have been conducted to reveal the actual physics/mechanism behind the transition of FSS/RSS and side-loads. Many researchers have presented the occurrence of lateral side-loads, but failed to explain the detailed mechanism for them. Also, the key parameters governing fluctuations remain unknown. Why do side-load fluctuations increase in the transition? Will these fluctuations be the same in different nozzle geometries? Answers to these questions have not been satisfactorily given. These unanswered questions are the motivation for the present work. Validation and reproduction of the known mechanisms are essential before taking up the actual work of finding answers to the questions above. In the present study, a computational fluid dynamic analysis of the transient flow during start-up was carried out to validate the previous findings from experiments. Side-loads were observed during the transition from FSS to RSS. In addition, the oscillatory phenomenon was observed at high pressure ratios. This work represents the first phase of investigations regarding the side-load fluctuations of rocket nozzles in start-up processes.

2. Governing equations

The flow simulation is based on the solution to Reynolds Averaged Navier-Stokes equations with Reynolds-stress closures for the corresponding Reynolds-stress transport equations.

$$\frac{\partial \boldsymbol{U}}{\partial t}+\frac{\partial\left(\boldsymbol{F}-\boldsymbol{F}_{v}\right)}{\partial x}+\frac{\partial\left(\boldsymbol{G}-\boldsymbol{G}_{v}\right)}{\partial y}=\boldsymbol{Q} \tag{1}$$

where:

$$\boldsymbol{U}=\begin{pmatrix}\rho\\ \rho u\\ \rho v\\ \rho\left(\dfrac{e+V^{2}}{2}\right)\\ \rho\overline{u_i'u_j'}\end{pmatrix},\ \boldsymbol{F}=\begin{pmatrix}\rho u\\ \rho u^{2}+p\\ \rho vu\\ \rho\left(e+\dfrac{V^{2}}{2}\right)u+pu\\ \rho\overline{uu_i'u'}_j\end{pmatrix},$$

$$\boldsymbol{F}_v = \begin{pmatrix} 0 \\ \tau_{ii} \\ \tau_{ij} \\ k_t \dfrac{\partial T}{\partial x} + u\tau_{ii} + v\tau_{ij} \\ -\rho\overline{u_i'u_j'u_k'} - p\left(\delta_{kj}u_i' + \delta_{ik}u_j'\right) + \mu\overline{\zeta_i} \end{pmatrix} \quad (2)$$

$$\boldsymbol{G} = \begin{pmatrix} \rho v \\ \rho uv \\ \rho v^2 + p \\ \rho\left(e + \dfrac{V^2}{2}\right)v + pv \\ \rho v\overline{u_i'u_j'} \end{pmatrix}, \quad \boldsymbol{Q} = \begin{pmatrix} 0 \\ 0 \\ 0 \\ 0 \\ P_{ij} + \phi_{ij} - \varepsilon_{ij} \end{pmatrix},$$

$$\boldsymbol{G}_v = \begin{pmatrix} 0 \\ \tau_{ji} \\ \tau_{jj} \\ k_t \dfrac{\partial T}{\partial y} + u\tau_{ji} + v\tau_{jj} \\ -\rho\overline{u_i'u_j'u_k'} - p\left(\delta_{kj}u_i' + \delta_{ik}u_j'\right) + \mu\overline{\zeta_j} \end{pmatrix} \quad (3)$$

where U is a conservation variable vector, F and G are inviscid flux vectors, and F_v and G_v are viscous flux vectors. Q is the source term corresponding to turbulence. $\overline{u_i'u_j'}$ is the Reynolds stress of the RSM model. In Eq. (1), t is the time, x and y are the space coordinates, ρ is the density, p the pressure, u and v are the components of fluid velocity, and e is the specific internal energy. These governing equations are closed by equations of state. In the Reynolds Stress Model (RSM) for modeling turbulence, $\overline{\zeta_i}$ is the molecular diffusion term, which is defined as:

$$\overline{\zeta_i} = \frac{\partial}{\partial x_k}\left(\overline{u_i'u_j'}\right) \quad (4)$$

where P_{ij} , ϕ_{ij} , and ϕ_{ij} are the production, dissipation, and pressure strain terms, respectively. These properties can be represented as:

$$P_{ij} = -\rho\left(\overline{u_i'u_k'}\frac{\partial u_j}{\partial x_k} + \overline{u_i'u_k'}\frac{\partial u_i}{\partial x_k}\right),$$
$$\phi_{ij} = \overline{p\left(\frac{\partial u_i'}{\partial x_j} + \frac{\partial u_j'}{\partial x_i}\right)}, \varepsilon_{ij} = 2\mu\overline{\frac{\partial u_i'}{\partial x_k}\frac{\partial u_j'}{\partial x_k}} \quad (5)$$

Among the various terms in these exact equations, P_{ij} does not require any modeling. However, ϕ_{ij} and ϕ_{ij} need to be modeled to close the equations.

3. Numerical procedure

Reynolds Averaged Navier-Stokes equations are numerically solved using a fully implicit finite volume scheme. Second order accuracy in space is achieved by using the upwind method. RSM is employed to close the governing equation systems, which are solved by a coupled implicit scheme. The RSM model is considered in the present work because it is the most elaborate turbulence model which considers the anisotropic eddy-viscosity hypothesis. It is appropriate for unsteady state calculations while other turbulence models are based on time-average treatments. It reflects the effects of streamline curvature, swirl, rotation, and rapid changes in strain rate in a more rigorous manner than one-equation and two-equation models.

The computational domain consists of a typical TOC nozzle as shown in Fig. 3. A TOC nozzle consists of r_e and r_i as the nozzle exit and inlet radii, respectively. The throat radius r_t considered was 0.01362 m and the length of the nozzle was approximately $15r_t$. The computational grid had 560 points in an axial direction (460 points inside the nozzle) and 121 points in a radial direction. Grid cells numbered more than 67,760. The total length of computational domain was $300r_t$ in the axial direction, and $40r_t$ in the radial direction. Boundary conditions considered at the inlet are total pressure (P_o) and total temperature (T_o). At the outlet boundary, static pressure (P_a) was given as the back pressure (Fig. 3). Air was chosen as the working substance and treated as an ideal gas. The wall was treated as a non-slip and adiabatic boundary. The viscous coefficient was calculated by Sutherland's formula. The mesh was clustered close to the nozzle wall in order to have a y^+ value less than 1.

A steady state pressure ratio (P_o/P_a) of 10.2 was considered at the beginning of the start-up process. The total pressure and temperature values at inlet were $P_o = 10.2\text{x}10^5$ Pa and $T_o = 270$ K, respectively. The computational domain was initialized by $P_a = 10^5$ Pa, $T_a = 288$ K with zero velocities. Steady state computations then used the previously computed flow field as an initial condition.

An unsteady calculation was carried out with a time step of 2×10^{-6} s by changing the flow boundary conditions. The pressure ratio was increased in the computational procedure of the

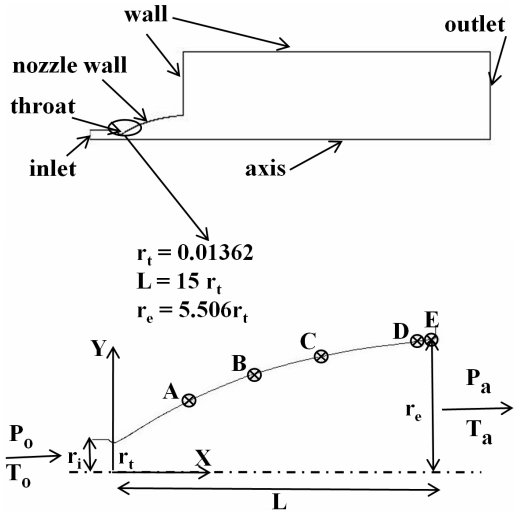

Fig. 3. Computational domain with boundary conditions and nozzle geometries.

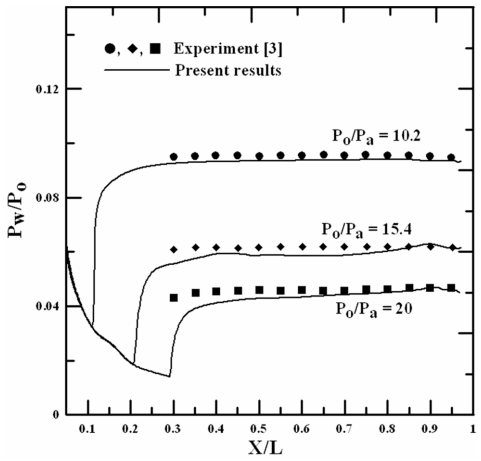

Fig. 4. Comparison of wall pressure distributions present along the nozzle wall.

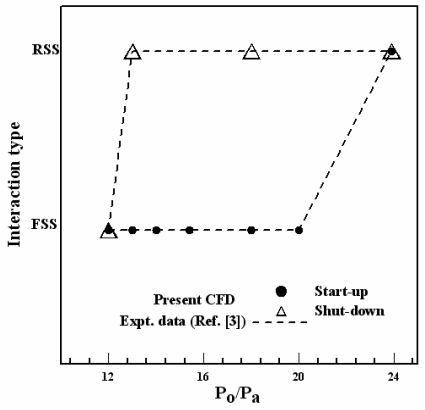

Fig. 5. Hysteresis cycle observed in present CFD.

start-up transient process, that is, it was increased by 1 for 1 ms to obtain a linear increment followed by a stabilization period of 9 ms. At a particular pressure ratio, the experiment was carried out for 10 ms. The computations were repeated until the desired pressure ratio was achieved.

A validation study was carried out for pressure ratios of 10.2, 15.4, and 20.0. Figure 4 shows the comparison of the wall pressure ($P_{w/}$ P_o) distributions present along the nozzle wall with the results of Nguyen et al. [3]. The present computational results show a good match with the experimental data.

4. Results and discussion

The FSS structure was observed for the pressure ratios 10.2, 15.4, 18 and 20.0. In FSS, the boundary layer separated, and never reattached to the nozzle wall (Fig. 1). The transition from FSS to RSS was seen by increasing the pressure ratio from 20.0 to 23.9. A cap-like shock structure, which generated during the increase in pressure ratio, forced the separated boundary layer to reattach to the nozzle wall (Fig. 2). The RSS pattern was obtained at a pressure ratio of 23.9 and by decreasing the pressure ratio from 23.9 to 18.0 to 13.0. The FSS pattern was again observed when the pressure ratio was decreased from 13.0 to 12.0. At these pressure ratios, the hysteresis cycle between the FSS and RSS was observed (Fig. 5). The present numerical calculations thus show the cycle of hysteresis in the pressure ranges of 12 to 23.9, against the range, demonstrated in experimental data, of 12 to 24 [3].

The transition of FSS to RSS occurred during the start-up process, when the pressure ratio was increased from 20.0 to 22.0. The pressure ratio was increased linearly in two steps. In the first step, the pressure ratio was linearly increased from 20.0 to 21.0 in 1 ms, followed by a stabilization period of 9 ms. The second step increased the linear increment of pressure ratio from 21.0 to 22.0 in 1 ms as shown in Fig. 6. At t = 0.001 s, FSS shock structure was observed, which corresponded to a pressure ratio of 20.0, and showed the absence of wall pressure (P_w) fluctuations. As the pressure ratio was linearly increased, the cap-shock pattern slowly appeared (Fig. 2). Initially, the pressure remained very close to the ambient pressure, P_a = 10^5 Pa, downstream to the shock structure (Fig. 7(a)). The shock structure moved downstream from the nozzle, as the pressure ratio increased. The separation point moved downstream because the static pressure was less than the ambient pressure in the recirculation bubble between the separation and reattachment points. The wall pressure at the nozzle exit increased to reach the external value P_a. Oscillations of wall pressure around P_a appeared at t = 0.0067 s and developed strongly in the reattaching region starting from t = 0.0075 s, as shown in Figs. 7(a) and 7(b).

These wall pressure fluctuations occurred due to the expansion and compression waves reflected between the wall and central recirculating vortex. The maximum wall pressure during this transition was observed to be close to 2.0×10^5 Pa. Wall pressure and wall shear stress profiles at Locations A, B, and C are shown in Figs. 8(a) and 8(b), where *Pw (t)* and τ_w *(t)* represent the time history of wall pressure and wall shear stress, respectively. *Pw (t),avg* and τ_w *(t),avg* are the average values over time t. Location A was at the upstream region of separation, while Locations B and C were at the downstream regions. Fluctuations in wall pressure and shear stress were observed during transition of FSS to RSS at Location A. Locations B and C, being at the downstream region of separation, did not show fluctuations. This high pressure value means that a small asymmetry of the flow can give important side-loads [16]. Thus, the origin of side-loads in thrust optimized nozzles is due to the transition of FSS to RSS.

In the present study, the behavior of nozzle wall pressure at a high pressure ratio was also studied. An unsteady numerical simulation was carried out at a high pressure ratio of 48.2. Numerical simulations were conducted for 0.05 s at this pressure ratio. Pressure variations were calculated at Locations D and E, which were at X/L = 0.905 and X/L = 0.944, respectively , X/L denotes the axial location (Fig. 3). At this high pressure ratio, the RSS pattern was observed. The time history of wall pressure P_w *(t)* at Locations D and E are shown in Figs. 9 and 10. Additionally, strong pressure variations were observed at these locations.

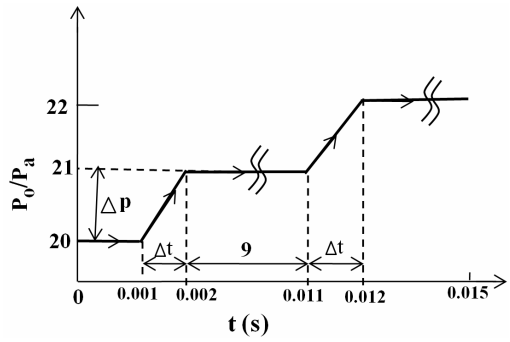

Fig. 6. Unsteady time variation plot for FSS/RSS transition simulation (Not up to scale).

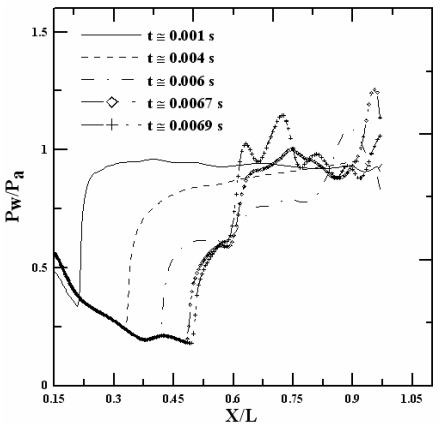

(a)

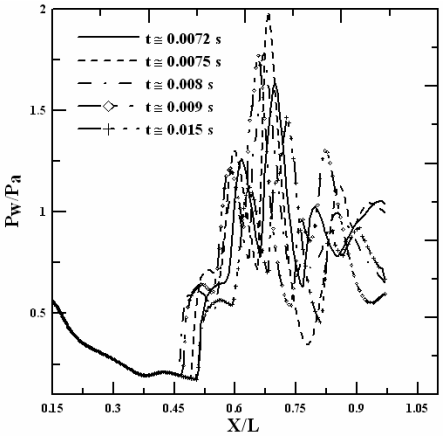

(b)

Fig. 7. Time dependent wall pressure distributions for the start-up process. Time proceeds from (a) t = 1 to t = 6.9 ms, and (b) t = 7.2 to t = 15 ms.

Location E, which was near the exit of the nozzle, showed more pressure peaks than those observed at D. Pressure oscillations were even seen at Location D, which was at X/L = 0.905. Thus, pressure oscillations were visible up to some axial distance from the nozzle wall exit. Fig. 11 presents the power spectral density (PSD) of the wall pressure shown in Figs. 10 and 11. The wall pressure fluctuations showed a peak

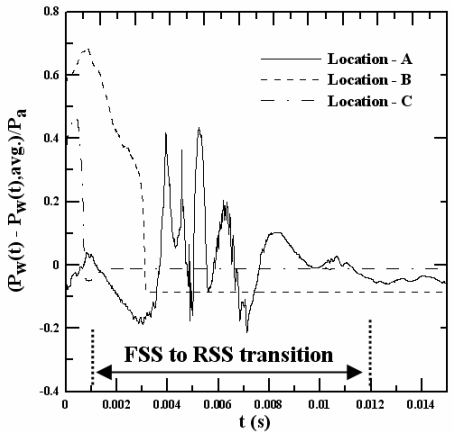

(a)

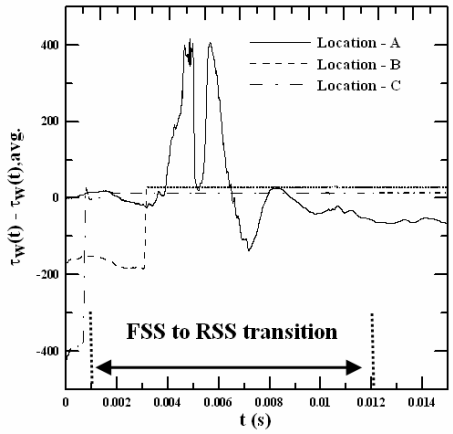

(b)

Fig. 8. Time dependent wall (a) pressure and (b) shear stress distributions for the start-up process.

located at about 550 Hz and 130 Hz for the Locations D and E, respectively. Hence, at high pressure ratio, pressure oscillations showed a high frequency for Location D and a low frequency for location E. The origin of the side load phenomenon was due to the appearance of the sudden peaks of wall pressure. The maximum value of unsteady wall pressure profiles was observed during the oscillatory phenomena (Figs. 9 and 10). Hence, the oscillatory phenomenon showed wall pressure peaks higher than those that appeared during the transition of FSS to RSS (Fig. 8(a)).

5. Conclusions

A numerical investigation of axisymmetric thrust-optimized contour nozzle flow separation was performed using the RSM turbulence model. The present computational results were in good agreement with experimental and other numerical data. The numerical simulations showed the occurrence of hysteresis between the free shock separation (FSS) and restricted shock separation (RSS) patterns. The transition from FSS to RSS patterns was numerically reproduced during the start-up process. Peaks in wall pressure were observed during the transition. Pressure oscillations on the nozzle wall were also ob-

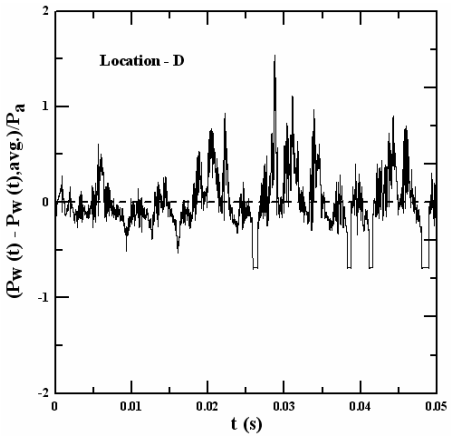

Fig. 9. Time dependent wall pressure during oscillatory phenomena at Location D (P_o/P_a = 48.2).

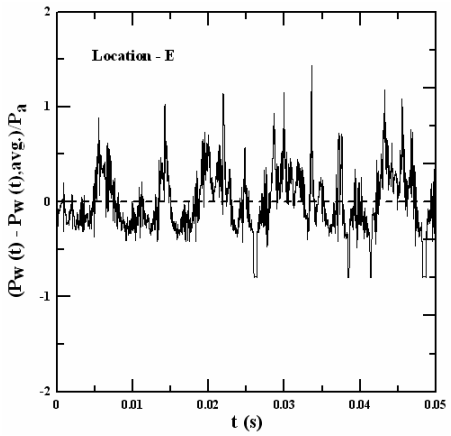

Fig. 10. Time dependent wall pressure during oscillatory phenomena at Location E (Po/Pa = 48.2).

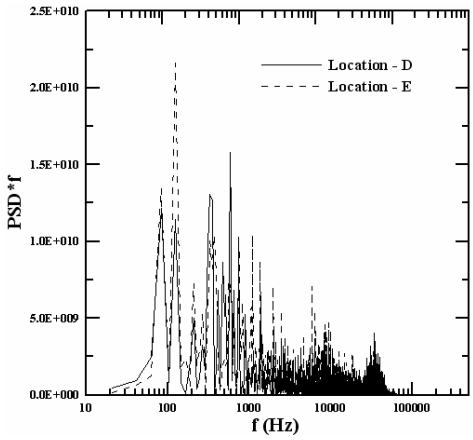

Fig. 11. Power spectral density plot of wall pressure oscillation at Locations D and E (P_o/P_a = 48.2).

served at high pressure ratios. These pressure oscillations were observed even at the upstream region of the nozzle. Low frequencies were observed near the nozzle wall exit, whereas high frequencies were observed at the upstream region of the nozzle. Finally, the magnitude of the wall pressure variation associated with the oscillatory phenomenon was greater than that associated with the transition from FSS to RSS patterns.

Acknowledgment

The authors would like to thank Korea Science and Engineering Foundation for financially supporting this research work under the Korea-Japan Basic Scientific Cooperation Program, No. F01-2009-000-10040-0.

References

[1] L. H. Nave and G. A. Coffey, Sea levels side loads in high-area-ratio rocket engines, *AIAA Paper* 73-1284 (1973).

[2] S. Nagdewe and H. D. Kim, A computational study on the unsteady lateral loads in a rocket nozzle, *proc. of Korean Society for propulsion Engineers*, KAIST, Daejeon, Korea (2008).

[3] A. T. Nguyen, H. Deniau, S. Girard and T. A. Roquefort, Unsteadiness of flow separation and end-effects regime in a thrust-optimized contour rocket nozzle, *Flow, Turbulence and Combustion*, 71 (2003) 161-181.

[4] C. L. Chen, S. R. Chakravarthy and C. M. Hung, Numerical investigation of separated nozzle flows, *AIAA Journal*, 32 (9) (1994).

[5] F. Nasuti and M. Onofri, Viscous and inviscid vortex generation during nozzle flow transients, *AIAA Paper 96-0076 (*1996).

[6] M. Onofri and F. Nasuti, The physical origins of side-loads in rocket nozzles, *AIAA Paper 99-2587* (1999).

[7] M. Frey and G. Hagemann, Status of flow separation prediction in rocket nozzles, *AIAA Paper 98-3619* (1998).

[8] M. Frey and G. Hagemann, Flow separation and side-loads in rocket nozzles, *AIAA 99-2815* (1999).

[9] F. Welsh, Electron beam fluorescence measurements of shock reflection hysteresis in an underexpanded supersonic jet, *proc. of the 21st International Symposium on Shock Waves,* Great Keppel Island, Australia, (1997).

[10] B. Gribben, F. Cantariti, K. Badcock and B. Richards, Numerical study of an under-expanded jet, *proc. of 3rd European Symposium on Aerothermodynamics of Space Vehicles, ESA-ESTEC*, Netherlands, (1998).

[11] G. Hagemann, M. Terhardt, M. Frey, P. Reijasse, M. Onofri, F. Nasuti and J. Ostlund, Flow separation and side-loads in rocket nozzles, *proc. of 4th International Symposium on Liquid Space Propulsion*, Lampoldshausen, Germany (2000).

[12] A. Nebbache and C. Pilinski, Pulsatory phenomenon in thrust-optimized contour nozzle, *Aerospace Science and Technology*, 10 (2006) 295-308.

[13] J. A. Morinigo and J. J. Salva, Three-dimensional simulation of the self-oscillating flow and side-loads in an over-expanded subscale rocket nozzle, *proc. of the I MECH E Part G Journal of Aerospace Engineering*, 220 (2006) 507-523.

[14] G. Hagemann and M. Frey, Shock pattern in the plume of rocket nozzle: needs for design consideration, *Shock Waves*,

17 (2008) 387-395.
[15] F. Nasuti and M. Onofri, Shock structure in separated nozzle flows, *Shock Waves*, DOI 10.1007/s00193-008-0173-7, published online, (2008).
[16] K. Yonezawa, T. Morimoto, Y. Tsujimoto, Y. Watanabe and K. Yokota, A study of an asymmetric flow in an overexpanded rocket nozzle, *Journal of Fluid Science and Technology*, 2 (2) (2007) 400-409.

Heuy-Dong Kim received his B.S. and M.S. degrees in Mechanical Engineering from Kyungpook National University, Korea, in 1986 and 1988, respectively. He then received his Ph.D. degree from Kyushu University, Japan, in 1991. Dr. Kim is currently a Professor at the School of Mechanical Engineering, Andong National University, Korea. His research interests include High-Speed Trains, Ramjet and Scramjet, Shock Tube and Technology, Shock Wave Dynamics, Explosions and Blast Waves, Flow Measurement, Aerodynamic Noises and Supersonic Wind Tunnels.

Vincent Lijo received B.Tech and M.Tech degrees in Mechanical Engineering from University of Kerala, India, in 1996 and 1998, respectively. He has been working as Assistant Professor in Mechanical Engineering, Government College of Engineering, Trivandrum, India. Presently he is on sabbatical leave, pursuing doctoral degree in School of Mechanical Engineering, Andong National University, Korea. His research interests include Supersonic Ejectors, Internal Flows, Cryogenics and Propulsion Engineering.